Article

Impact of Dy$_2$O$_3$ Substitution on the Physical, Structural and Optical Properties of Lithium–Aluminium–Borate Glass System

Osama Bagi Aljewaw [1], Muhammad Khalis Abdul Karim [1,](ID), Halimah Mohamed Kamari [1], Mohd Hafiz Mohd Zaid [1] (ID), Noramaliza Mohd Noor [2], Iza Nurzawani Che Isa [3] and Mohammad Hasan Abu Mhareb [4,5] (ID)

[1] Department of Physics, Faculty of Science, Universiti Putra Malaysia, Serdang 43400, Selangor, Malaysia; os.aljewaw@gmail.com (O.B.A.); halimahmk@upm.edu.my (H.M.K.); mhmzaid@upm.edu.my (M.H.M.Z.)

[2] Department of Radiology, Faculty of Medicine, Universiti Putra Malaysia, Serdang 43400, Selangor, Malaysia; noramaliza@upm.edu.my

[3] Diagnostic Imaging and Radiotherapy Programme, Faculty of Health Sciences, Universiti Kebangsaan Malaysia, Kuala Lumpur 50300, Malaysia; zawaniisa@ukm.edu.my

[4] Department of Physics, College of Science, Imam Abdulrahman Bin Faisal University, P.O. Box 1982, Dammam 31441, Saudi Arabia; mhsabumhareb@iau.edu.sa

[5] Basic and Applied Scientific Research Center, Imam Abdulrahman Bin Faisal University, P.O. Box 1982, Dammam 31441, Saudi Arabia

* Correspondence: mkhalis@upm.edu.my

check for updates

Abstract: In this study, a series of Li$_2$O-Al$_2$O$_3$-B$_2$O$_3$ glasses doped with various concentrations of Dy$_2$O$_3$ (where x = 0.0, 0.2, 0.4, 0.6, 0.8, and 1.0 mol%) were prepared by using a conventional melt-quenching technique. The structural, physical and optical properties of the glasses were examined by utilising a variety of techniques instance, X-ray diffraction (XRD), UV–Vis-NIR spectrometer, Fourier transform infrared (FTIR) and photoluminescence (PL). The XRD spectra demonstrate the amorphous phase of all glasses. Furthermore, the UV-vis-NIR spectrometers have registered optical absorption spectra a numbers of peaks which exist at 1703, 1271, 1095, 902, 841, 802, 669, 458, 393 and 352 nm congruous to the transitions from the ground of state ($^6H_{15/2}$) to different excited states, $^6H_{11/2}$, $^6F_{11/2}$ + $^6H_{9/2}$, $^6F_{9/2}$ + $^6H_{7/2}$, $^6F_{7/2}$, $^6F_{5/2}$, $^6F_{3/2}$, $^4F_{9/2}$, $^4I_{15/2}$, $^4F_{7/2}$ and $^6P_{7/2}$, respectively. The spectra of emission exhibit two strong emanation bands at 481 nm and 575 nm in the visible region, which correspond to the transitions $^4F_{9/2} \rightarrow {}^6H_{15/2}$ and $^4F_{9/2} \rightarrow {}^6H_{13/2}$. All prepared glass samples doped with Dy$_2$O$_3$ show an increase in the emission intensity with an increase in the concentration of Dy^{3+}. Based on the obtained results, the aforementioned glass samples may have possible applications, such as optical sensor and laser applications.

Keywords: borate glass; Dy$_2$O$_3$; UV-VIS-NIR; photoluminescence

1. Introduction

Borate glass has been acknowledge as a good host for various rare-earth (RE) oxides among the traditional glass formers due to their strong glass formulation when compared with other conventional systems such as phosphates, germanates, vanadates and tellurite glass [1]. In addition, the glassy system is available easily, inexpensive, simple to prepare and a good host for a variety of elements [2]. The structural, physical, and optical characteristics of the glasses are greatly influenced by the composition and synthesis conditions. Therefore, to accomplish high emission efficiency, most of the glass system is activated using suitable transitional metals and/or rare-earth elements.

The incorporation of rare-earth ions to the different glassy systems led to an improvement in the optical properties, such as refractive index, optical band gaps energy and laser amplification [3]. These improvements in optical properties for glassy systems drove them to be a potential candidate for lasers, solar concentrate systems, optical detectors, waveguides and telecommunications optical fibres [4].

Borate glasses have specific properties that make them beneficial for a wide technical application, but their chemical durability is relatively feeble, which limits their utility. Nevertheless, the addendum of oxides such as lithium oxide (Li_2O) and aluminium oxide (Al_2O_3) can enhance the chemical durability and physical properties. Moreover, adding metal oxides as modifiers to the host matrix raises the radiative parameters. Besides, glasses containing metals minimize phonon energy and lead to an increase in the luminescence quantum from excited rare-earth ion states [5]. Therefore, glasses doped with rare-earth elements may be used because of their ion emission efficiencies of 4f–4f and 4f–5d. The 5s and 5p orbits provide shielding effects to electrons determined by 4f, which leads to significant RE spectral absorption and emission lines [6,7]. Due to their unique characteristics, glass systems doped with rare-earth elements have been given considerable attention in recent decades.

Furthermore, between all the RE ions, trivalent dysprosium (Dy^{3+}) ions have been extensively investigated for the production of or improvement in optical amplification systems in telecommunication. It is important to study the luminescence of Dy^{3+} ions in level $^4F_{9/2}$ because it occurs in visible and NIR regions [8,9]. Usually, transitions of Dy^{3+} ion exhibit in yellow or blue regions of $^4F_{9/2} \rightarrow {}^6H_{13/2}$ (electric dipole) and $^4F_{9/2} \rightarrow {}^6H_{15/2}$ (magnetic dipole), respectively [10,11]. It has been established that the transition of $^4F_{9/2} \rightarrow {}^6H_{13/2}$ is hypersensitive, and therefore, its intensity depends heavily upon the existence of the host, while the intensity of transition of $^4F_{9/2} \rightarrow {}^6H_{15/2}$ is not quite sensitive to host conditions. Dy^{3+} has been acknowledged for its white light production, which is appropriate at an acceptable yellow to blue (Y/B) intensity ratio. Luminescent materials doped by Dy^{3+} ions are therefore commonly used both in glasses and phosphors to generate white light [5,6,10]. Moreover, Dy^{3+} ions have a various interesting characteristics such as high mechanical strength, high sensitivity and high thermal neutron absorption. They also can be utilized as the X-ray scintillators and as a yellow laser medium due to their intense yellow emission [12–14]. Unfortunately, there is limited information on the structure and physical properties of aluminium borate-bases doped with rare-earth ions, especially with Dy^{3+} ion. Hence, in this study, we seek to examine the impact of dysprosium oxide (Dy_2O_3) on the physical, structural and optical properties of $23Li_2O$-$(69.5 - x)$ B_2O_3-$7.5Al_2O_3$: xDy_2O_3 glass series (where x = 0, 0.2, 0.4, 0.6, 0.8 and 1 mol%).

2. Materials and Methods

2.1. Glass Preparation

The new glass formulation was prepared by using the conventional melt-quench technique. Various raw materials such as lithium oxide (Li_2O), aluminium oxide (Al_2O_3), boron oxide (B_2O_3) and trivalent dysprosium oxide (Dy_2O_3) were chosen at a specific ratio, as illustrated in Table 1. The chemical powders were weighed and mixed well for 60 min at 90 rpm. Then, the mixture was put in an alumina crucible and inserted in an electrical furnace for 30 min to be melted at 1000 °C to ensure complete melting. After that, the mixture was moved to another furnace for annealing at 400 °C for three hours. Then, the temperature of the furnace decreased progressively to reach the ambient temperature at a cooling rate of 10 °C per minute. Lastly, the samples were divided into two groups, where the first group was grinded to explore the characterisation, and the second group was buffed to investigate the optical of properties.

Table 1. Composition ratios for all studied glass samples.

Glass Samples	mol%			
	Li$_2$O	Al$_2$O$_3$	B$_2$O$_3$	Dy$_2$O$_3$
LABD-0.0	23	7.5	69.5	0.0
LABD-0.2	23	7.5	69.3	0.2
LABD-0.4	23	7.5	69.1	0.4
LABD-0.6	23	7.5	68.9	0.6
LABD-0.8	23	7.5	68.7	0.8
LABD-1	23	7.5	68.5	1

2.2. Structural and Physical Parameters

The weight of the prepared glass samples was measured in air and distilled water using a sensitive microbalance based on the Archimedes principle. The density, ρ, of the samples was calculated by using the following equation

$$\rho = \left(\frac{W_A}{(W_A - W_B)} \right) * \rho_B \tag{1}$$

where W_A and W_B denote the sample weight in the air and distilled water, respectively, and ρ_B is the density of distilled water, $\rho_B = 0.999 gcm^{-3}$. Molar volumes (V_m) for all glass samples were determined using the following equation

$$V_m = (M_{av}/\rho)(cm^3/mol) \tag{2}$$

where M_{av} represents the average molecular weight. The average boron–boron separation $\langle d_{B-B} \rangle$ was calculated by applying the following formula

$$\langle d_{B-B} \rangle = \left[V_m^b/N_A \right]^{\frac{1}{3}} \tag{3}$$

where V_m^b refers to the volume of boron atoms per mole and is given by

$$V_m^b = V_m/2(1 - X_B) \tag{4}$$

where X_B is the mole fraction and V_m is Molar volume for the glass samples [15]. The ion concentration can be acquired using the next expression

$$N = \left(\frac{X\% * \rho * N_A}{M_T} \right) \left(\frac{ion}{cm^3} \right) \tag{5}$$

where $X\%$ is the mole percent of dopant, N_T is the Avogadro number, and M_T is the molecular weight. Based on the ion concentrations, it is also possible to compute three essential physical parameters, such as Polaron radius (r_p), inter-nuclear distance (r_i) and field strength

$$r_p(A°) = \frac{1}{2} \left[\pi/6N \right]^{\frac{1}{3}} \tag{6}$$

$$r_i(A°) = \left[1/N \right]^{\frac{1}{3}} \tag{7}$$

$$F = \left(\frac{Z_m}{r_P^2} \right) \tag{8}$$

where Z_m is the atomic mass of the dopant [16,17].

The non-crystalline phases for the selected samples were observed using X-ray diffraction (XRD) system PANalytical X'pert PRO (PW3040/60 MPD, Philips, EA, The Netherland). The system was combined with the software of diffraction analysis based on the 2θ range from 10° to 80° with the steps 0.02°. Perkin Elmer Spectrum 100 (Waltham, MA, USA) instrument was utilized to obtain the

FTIR spectrum absorption for studied glasses with the size <63 μm in Attenuated-Total Reflectance (ATR) mode within wavenumber range of 400–4000 cm^{-1}.

2.3. Optical Properties

2.3.1. UV-Vis-NIR Absorption Spectra

UV-Vis spectrophotometer for reflective spectroscopy (RSA) (Lambda 35 Perkin Elmer, MA, USA) was used to estimate the absorption spectra of the glass samples within wavelength ranges of 200–2600 nm. Using absorption, the energy gap (E_g) can be obtained by applying the Mott and Davis relation

$$(\alpha h\nu) = A\left(h\nu - E_g\right)^n / (h\nu)$$ (9)

where α is coefficient of optical absorption, A is a constant, ($h\nu$) is the incident photon energy, and E_g is the indirect permitted optical band gap energy. The direct E_g value is obtained from the plot $(\alpha h\nu)^{1/2}$, and $h\nu$ by extrapolating the linear-compatible regions to the value $(\alpha h\nu)^{1/2} = 0$ [16]. Urbach energy (E_u) offers knowledge about glass disorder. This E_u can be measured by using the relation [8]

$$\alpha(\nu) = c.\exp\left(h\nu/E_u\right)$$ (10)

where c is constant and E_u is Urbach energy. The oscillator strength $\left(f_{\exp}\right)$ of glasses can be determined using the next equation

$$f_{\exp} = 4.32 * 10^{-9} \int \varepsilon(\nu)d\nu$$ (11)

where $\varepsilon(\nu)$ is the coefficient of molar the absorption of the each band at an energy of $\nu(\text{cm}^{-1})$ [17–19]. The refractive index (n) for the electronic polarization of ions and the local field of materials is among the most important optically dependent material parameters. The next relation can be used to define the refractive index (n)

$$\frac{\left(n^2 - 1\right)}{(n^2 + 2)} = 1 - \frac{\sqrt{E_g}}{20}$$ (12)

Reflective loss on the surface of the glass is determined by using the refractive index of the Fresnel formula

$$R_L = \left(\frac{(n-1)}{(n+1)}\right)^2$$ (13)

Using the Volf and Lorentz–Lorenz formula, the molar refraction (R_m) for all samples was measured [20,21]

$$R_m = \left(\frac{\left(n^2 - 1\right)}{(n^2 + 2)}\right) * V_m$$ (14)

Molar refractivity (R_M) can be acquired using the following equation [22]

$$R_m = \frac{\left(n^2 - 1\right)}{(n^2 + 2)} * \left(\frac{M}{\rho}\right)$$ (15)

The following relation can be used to estimate molar polarizability (α_m) [23]

$$\alpha_m = \left(3/4\pi N_A\right) * R_m$$ (16)

Metallisation criterion is the prediction of the metal or isolating behaviour of the condensed matter and is determined using the following relation [24]

$$M = 1 - \left(\frac{R_m}{V_m}\right) \tag{17}$$

The materials are considered metallic when $R_m/V_m > 1$, and they are considered insulating when $R_m/V_m < 1$. Further, the polarizability of electrons (α_o) and optical basicity (Λ) linked electronegativity (χ) can be obtained by [25]

$$\chi = 0.2688E_g \tag{18}$$

where (E_g) is optical band gap. The electronic polarizability is given by

$$\alpha_\circ = -0.9\chi + 3.5 \tag{19}$$

The relation between the electronic oxide polarizability and optical basicity is described by [26].

$$\Lambda = 1.67(1 - \frac{1}{\alpha_{2-}}) \tag{20}$$

The dielectric constant (ε) and optical dielectric constant can be calculated using the following formulae [8]. The dielectric constant has calculated using refractive index of the glass

$$\varepsilon = n^2 \tag{21}$$

where (n) is the refractive index. The optical dielectric constant of the glass calculated by the following relation

$$p\frac{dt}{dp} = (\varepsilon - 1) = n^2 - 1 \tag{22}$$

where ε is the dielectric constant.

2.3.2. Photoluminescence (PL) Spectrum

The LS55 Luminescence Spectrophotometer (Perkin Elmer, MA, USA) was used to determine photoluminescence between the wavelengths of 200 and 1300 nm. The luminescence signal was analysed based on excitation and emission methods using a Monk–Gillieson monochromator.

3. Results and Discussion

The pattern of the XRD for all the glass samples did not show any sharp diffraction or peaks, as shown in Figure 1, which confirms the amorphous nature for all the studied glass samples. Figure 2 shows the FTIR spectrum for lithium–aluminium–borate (LAB) glass doped with various Dy^{3+} ion concentrations. All infrared spectrums revealed several absorption bands, as listed in Table 2.

Density (ρ) is a key physical parameter for analysing the physical features of glass samples, as it indicates the relation between the masses and the volume within the glass system. Likewise, the molar volume (V_m) also correlates directly to the oxygen distribution in the glass structure. Figure 3 shows the relation between the density and molar volume of the glass upon adding the different concentrations of Dy_2O_3.
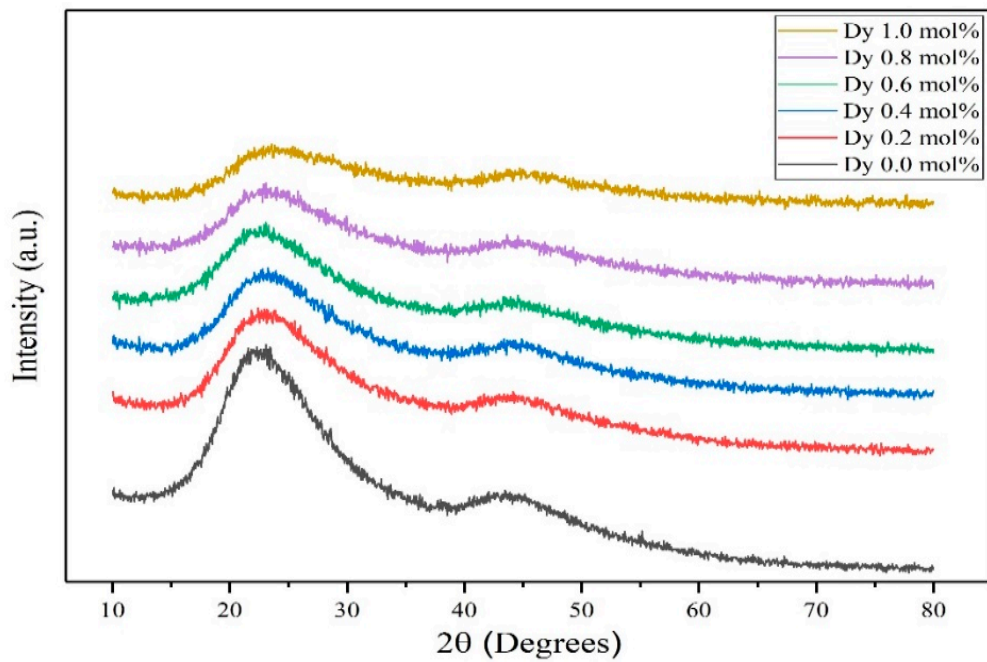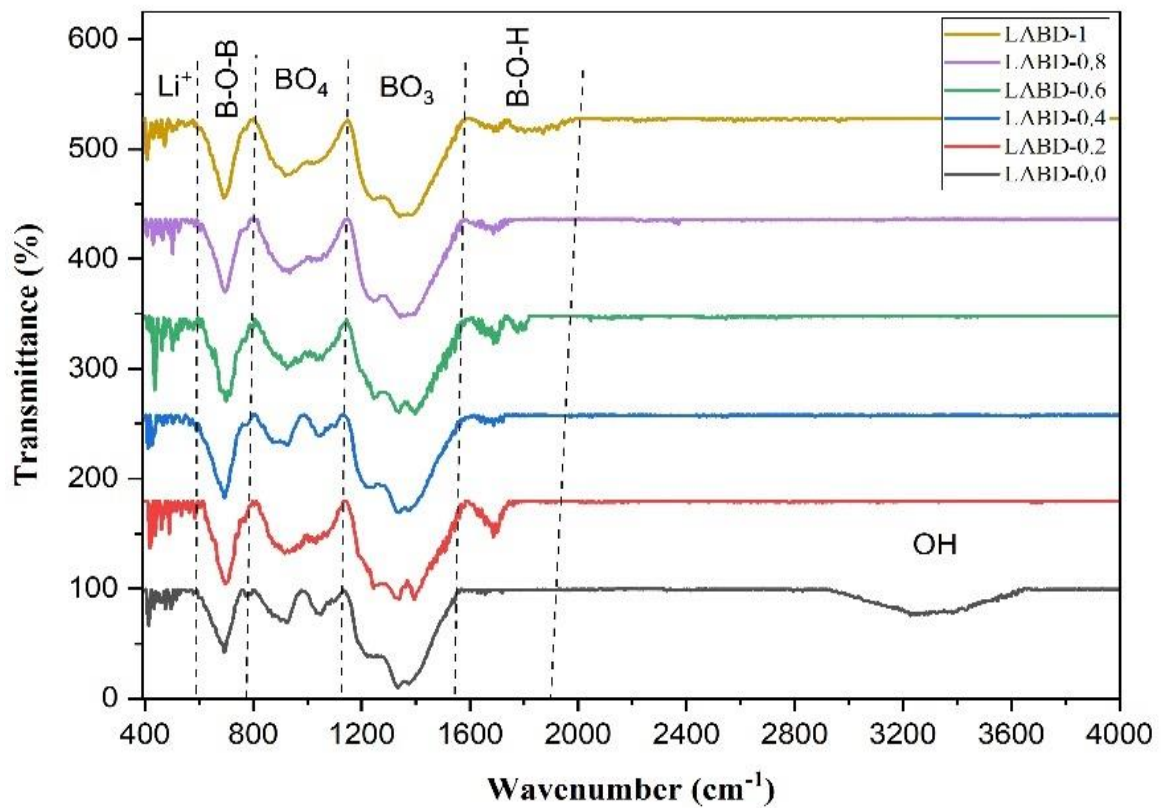
Figure 1. XRD pattern for all studied glasses.

Figure 2. FTIR of spectra for the various concentration of Dy^{3+} doped in $Li_2O–Al_2O_3–B_2O_3$ glasses.

Table 2. FTIR assignment bands of Li_2O–Al_2O_3–B_2O_3: Dy_2O_3 glasses.

| Positions of Band (cm^{-1}) for LAB Glasses with Diverse Dy^{3+} Ions Contents (mol%)						Band Assignments
0.0	0.2	0.4	0.6	0.8	1.0	
412.7, 526.5	416.6, 586.3	426.2, 540.06	433.9, 578.6	406.6, 588.3	406.9, 563.2	Vibrations of Li^+ ions [6].
692.4	696.3	694.3	700.1	696.3	692.4	Bending vibration B-O-B linkages with BO_3 units altogether with B-O-B bending vibration of bridging oxygen's in BO_3 and bonds in AlO_6 groups [27].
925.8, 1051.2	918.1, 1056.9	925.8, 1043.4	923.9, 1055.06	933.5, 1033.8	920.05, 1024.2	B-O stretching of tetrahedral BO_4 bond [10].
1227.9, 1334.7, 1375.2	1244.09, 1332.8, 1396.4	1236.3, 1340.5, 1375.2	1246.02, 1328.9, 1390.6	1246.2, 1377.1	1247.9, 1382.9	B–O–, stretching in pyroborate units Stretching of the trigonal BO_3 units [8].
	1687.7	1687.7	1687.7, 1801.5	1687.7	1687.7, 1870.9	B-O-H bridge, OH bending vibration [28].
3269.3	–	–	–	–	–	Stretching of OH groups or O-H (H_2O bond) [29].
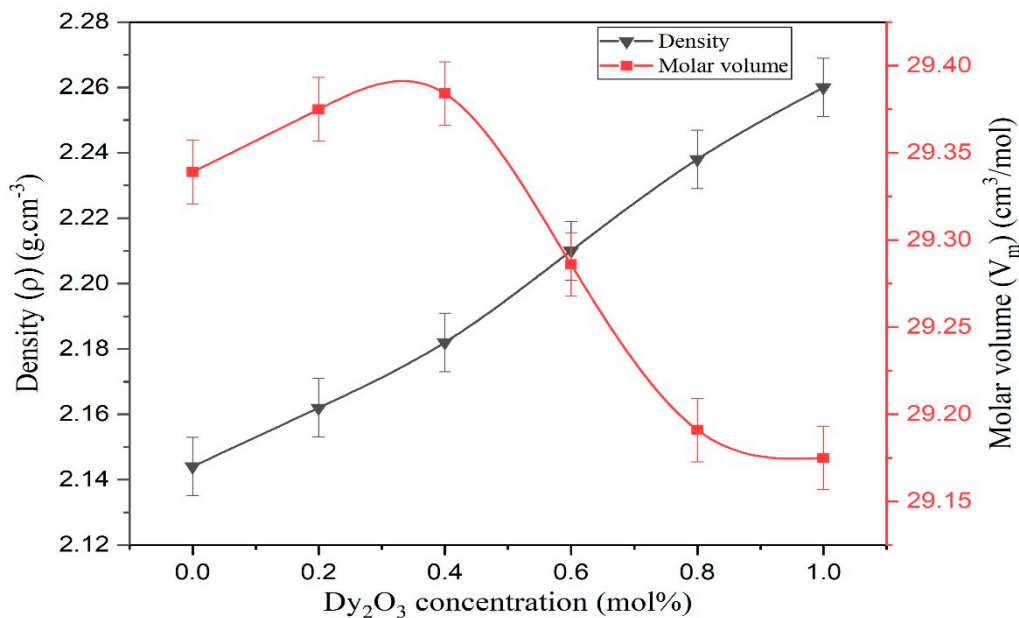
Figure 3. Variation in density (ρ) and molar volume (V_m) concerning Dy_2O_3.

As illustrated in Table 3, the V_m of these glasses increases slightly with increasing Dy_2O_3 concentration up to 0.4 mol%, but the V_m values decrease gradually from 29.28 up to 29.17 cm^3 with the addition of Dy_2O_3 up to 1 mol%. This enhancement in V_m value can be related to the decrement in glass compactness. Upon further addition of Dy_2O_3, the V_m values reduce gradually as a result of the increasing compactness of the glass system [27–29]. The replacement with Dy_2O_3 instead of B_2O_3 changes the ratio of boron to oxygen, creating BO_4 units that contribute to the compactness of the glass structure, thereby increasing the glass density. Furthermore, the molecular weight of Dy_2O_3 is higher than B_2O_3, meaning a significant increase in glass density [30].

Table 3. Physical properties for all series of glasses.

Physical Parameters *	Units	Doping (mol% Dy$_2$O$_3$)					
		0.0	0.2	0.4	0.6	0.8	1
Density	(g.cm^{-3})	2.144	2.162	2.182	2.210	2.238	2.260
Molecular weight, M$_T$	g	62.903	63.509	64.116	64.723	65.330	65.937
Molar volume V_m	(cm^3/mol)	29.339	29.375	29.384	29.286	29.191	29.175
The volume of boron atoms per mole V_m^b		16.031	11.959	11.886	11.058	11.656	11.576
Ion concentration (N) $\times 10^{20}$	(ions/cm^3)		0.410	0.819	1.233	1.650	2.064
Polaron radius (r_p) $\times 10^{-8}$			11.687	9.279	8.096	7.347	6.819
Inter-nuclear distance (r_i) $\times 10^{-8}$			29.0004	23.027	20.091	18.232	16.921
Field strength (F) $\times 10^{16}$	(cm^{-2})		1.189	1.887	2.479	3.010	3.494
Average of boron-boron distance ‹d$_{B-B}$›	nm	0.298	0.270	0.270	0.263	0.268	0.267

* With consideration of ± 0.01% error.

The calculated r_p, r_i and *F* values are listed in Table 3, and Figure 4 displays the behaviour of these parameters. The decrease in r_p and r_i with increased Dy$_2$O$_3$ is related to the decrease in the Dy–O distance, as a result of which the strength of the Dy–O bond increases, producing stronger field around Dy^{3+} ions [8]. Besides, the addition of Dy$_2$O$_3$ to the glass network led to overcrowding that decreased the average distance between the RE-oxygen. The significant increment in field strength values is, therefore, due to the appearance of strong linkages in the glass matrix between Dy^{3+} and B ions. [10]. It is noted from this table that the boron–boron separation ‹d$_{B-B}$› decreases with an increase in the Dy$_2$O$_3$ concentration due to the stretching force of the binds in the glass network.
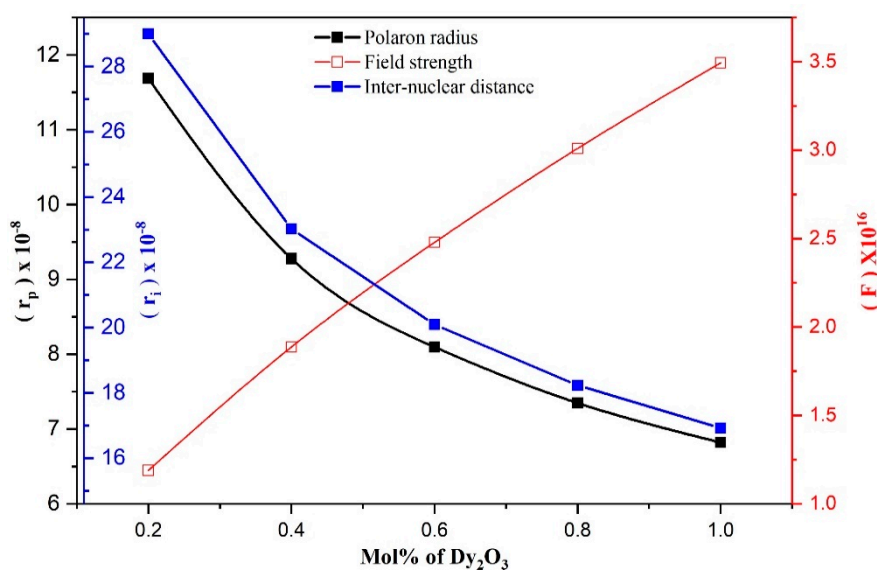

Figure 4. Polaron radius, inter-nuclear distance and field strength as functions of Dy$_2$O$_3$ content of prepared glasses.

Figure 5 displays the optical absorption spectrum for the Dy^{3+} doped lithium–aluminium–borate (LAB) glass samples within wavelengths in the range 300–1890 nm at room temperature. A spectrum identifies that the intensity of absorption raises with an addendum to Dy$_2$O$_3$ [29,31].
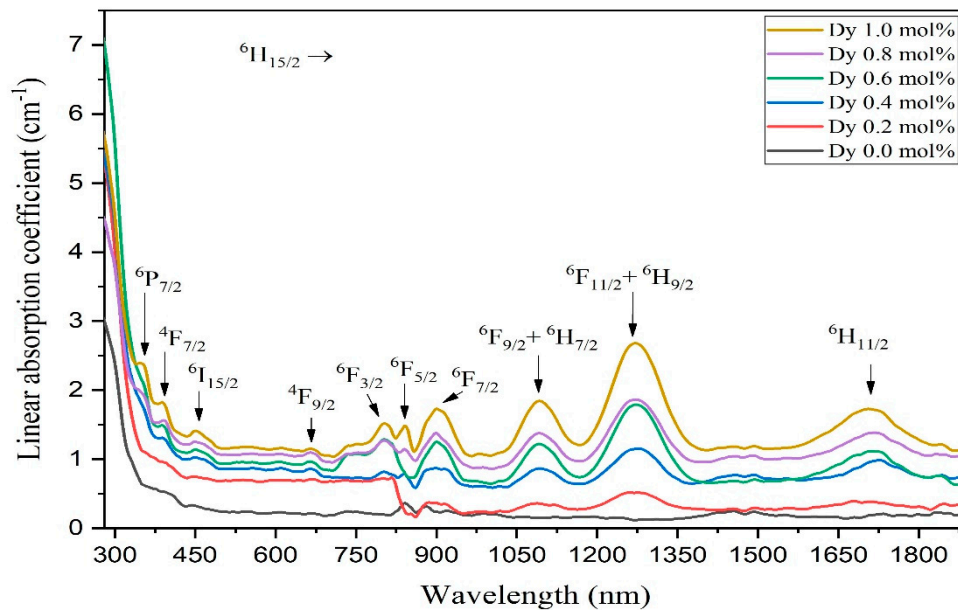
Figure 5. UV–Vis-NIR optical absorption spectra of different concentrations of Dy^{3+}-doped LAB glasses.

The spectra show ten inhomogeneous of absorption bands existing at the wavelengths 352, 393, 458, 669, 802, 841, 904, 1095, 1271 and 1703 nm due to the transitions of Dy^{3+} at the ground state ($^6H_{15/2}$) into different excited states ($^6P_{7/2}$), ($^4F_{7/2}$), ($^4I_{15/2}$), ($^4F_{9/2}$), ($^6F_{3/2}$), ($^6F_{5/2}$), ($^6F_{7/2}$), ($^6F_{9/2} + {}^6H_{7/2}$), ($^6F_{11/2} + {}^6H_{9/2}$) and ($^6H_{11/2}$), respectively [17]. Due to the strong absorption of LAB host glass, some of the absorption bands have disappeared in ultraviolet (UV) regions and are very sparse at 352 nm ($^6H_{15/2} \rightarrow {}^6P_{7/2}$), 393 nm ($^6H_{15/2} \rightarrow {}^4F_{7/2}$) and 456 nm ($^6H_{15/2} \rightarrow {}^4I_{15/2}$), and also they have very low intensity [32]. Besides, the current samples showed a hypersensitive transition at 1270 nm ($^6H_{15/2} \rightarrow {}^6H_{11/2}$) with high intensity and were subjected to the rule of selection $|\Delta S| = 0$, $|\Delta L| \leq 2$, and $|\Delta J| \leq 2$, where these transitions are more sensitive than others [33]. The variation between transition levels and their respective oscillator of strength for the glass samples are tabulated in Table 4. Noting that, the influence of Dy^{3+} ion on difference absorption bands led to their appropriate wavelengths, energies and oscillator strengths [34].

Table 4. The difference at transition levels and oscillator strengths.

Absorption Transition	Wavelength (nm)	Energy ($\times 10^{-3} cm^{-1}$)	Oscillator Strength f_{exp} ($\times 10^{-6}$)
$^6H_{15/2} \rightarrow {}^6P_{7/2}$	352	29.321	0.451
$^6H_{15/2} \rightarrow {}^4F_{7/2}$	393	25.945	0.520
$^6H_{15/2} \rightarrow {}^4I_{15/2}$	458	22.234	0.696
$^6H_{15/2} \rightarrow {}^4F_{9/2}$	669	13.523	0.554
$^6H_{15/2} \rightarrow {}^6F_{3/2}$	802	12.644	0.615
$^6H_{15/2} \rightarrow {}^6F_{5/2}$	841	11.113	0.478
$^6H_{15/2} \rightarrow {}^6F_{7/2}$	902	10.145	1.305
$^6H_{15/2} \rightarrow {}^6F_{9/2} + {}^6H_{7/2}$	1095	9.267	1.821
$^6H_{15/2} \rightarrow {}^6F_{11/2} + {}^6H_{9/2}$	1271	7.834	3.218
$^6H_{15/2} \rightarrow {}^6H_{11/2}$	1703	3.533	3.046

Figure 5 illustrate the optical energy band gaps for direct and indirect based on the curves of the UV-absorption spectrum. Figure 6a and 6b show the indirect and direct bandgap, respectively. The energy band gap value can be obtained by using Equation (9) to plot $(\alpha h v)^n$ against photon energy (hv). Then, the linear extrapolating region of the curves extending to the X-axis gives the energy bandgap (E_g) reading. In the recent glass system, the values of the direct E_g exhibit from 3.650

to 3.706 eV, and the values of indirect (E_g) show a decrease from 3.189 to 2.556 eV with increasing dopant contents, as listed in Table 5. The declines in E_g values may be due to structural changes due to the addition of Dy^{3+} ions. The addition of Dy_2O_3 can contribute to an increase in electron localisation that increases donor centres in the glass matrix. This increment causes a decrease in E_g values [35]. This is also because a new extrinsic band is formed by Dy^{3+} on the grid between the boron and oxygen ions. As a consequence, there is an amount of possible reduction in (B–O–B) [36].

(**a**)

(**b**)
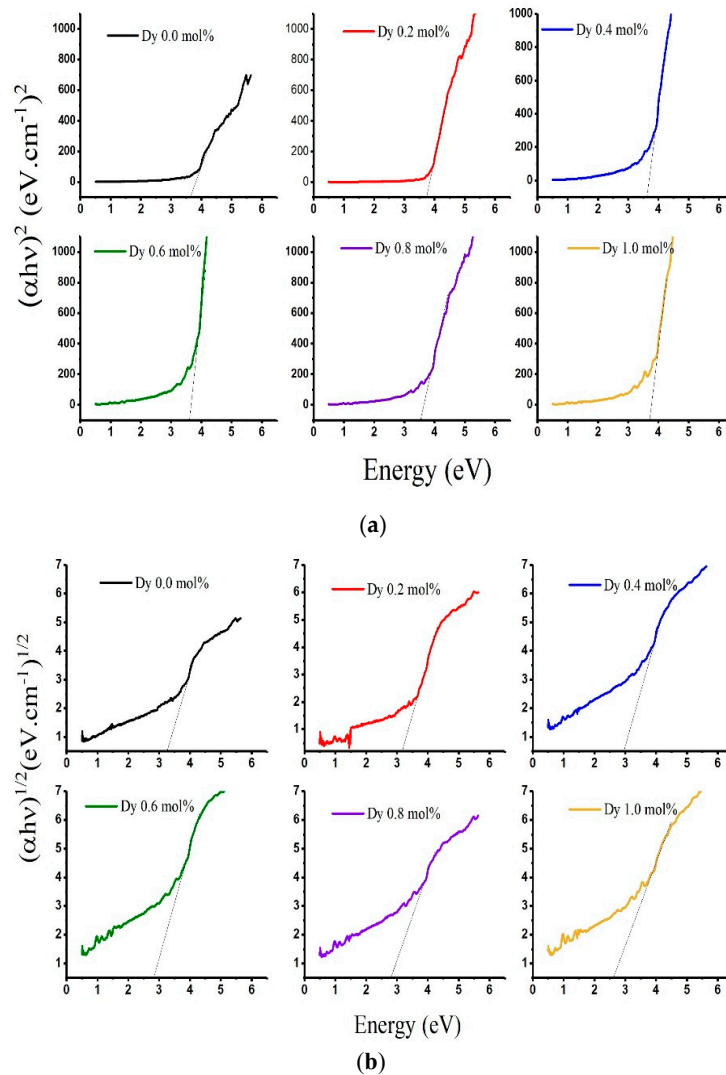
Figure 6. Bang gap energy: (**a**) Tauc's plot for allowed direct transitions (*n* = 2); (**b**) Tauc's plot for allowed indirect transitions (*n* = 1/2).

Table 5. Direct and indirect band gaps, Urbach energy (E_u) and cut-off wavelength (λ_c) of the samples studied.

Sample	E_{dir} (eV)	E_{indir} (eV)	E_u (eV)	λ_c [nm]
LABD-0.0	3.580	3.189	3.520	362.36
LADB-0.2	3.706	3.166	3.337	368.83
LABD-0.4	3.566	2.919	3.272	376.44
LABD-0.6	3.585	2.886	3.075	385.81
LABD-0.8	3.473	2.7005	3.352	394.15
LABD-1	3.650	2.556	3.058	401.81

Figure 7 indicates that the energy of Urbach decreases with changes in the Dy_2O_3 concentration. The reduction in the energy of Urbach is attributed to the creation of fewer defects, as reported [37]. Figure 8 and Table 6 show a slight gradual increase in refractive index values from 2.29 to 2.35 with increasing Dy_2O_3 concentration that can be attributed to the increase in electronic polarizability from 2.67 to 2.75 [17]. The sample has a higher refractive index, as it has a smaller bandgap value that reflects the compactness of the glass network structure. Meanwhile, the increment in molar refractivity and electronic polarisation values with increasing Dy_2O_3 concentration is indicated to form more non-bridging oxygen (NBOs) in the glass matrix [12].
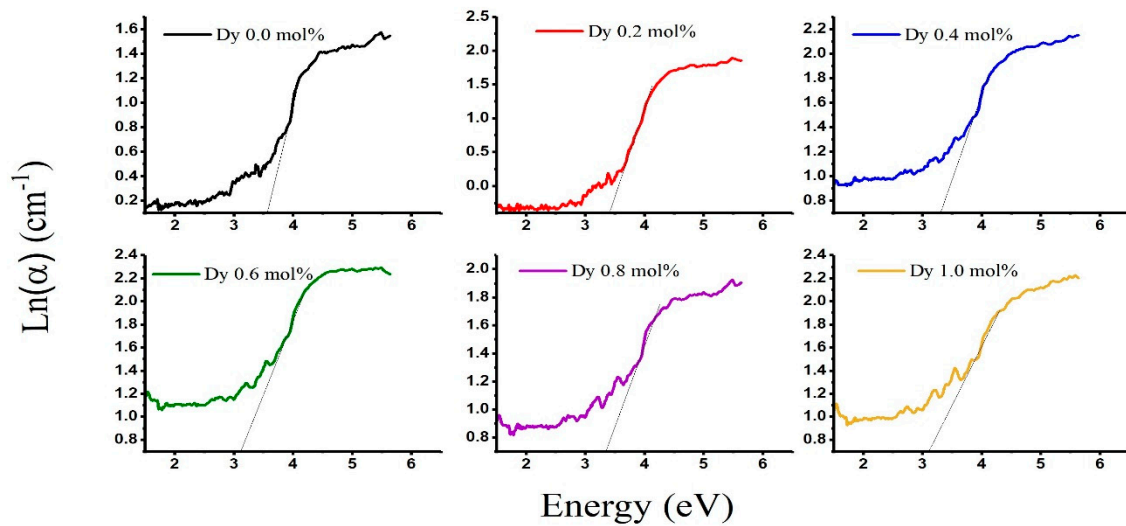
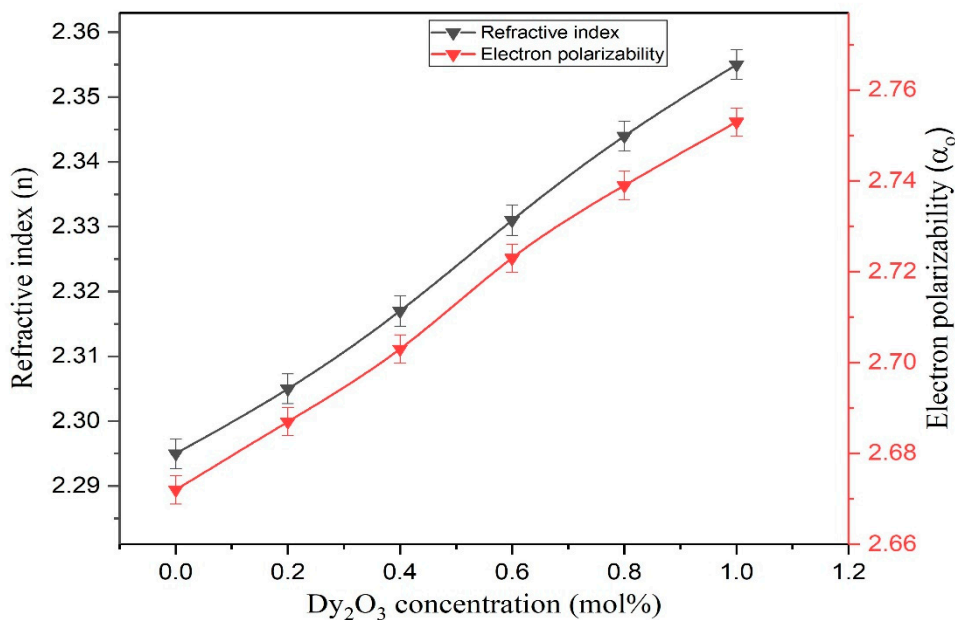**Figure 7.** Variation of Urbach energy (eV) with mol% of Dy_2O_3.

Figure 8. Variation in refractive index (*n*) and Electron polarizability (α_o) with concerning Dy_2O_3.

Table 6. Optical properties of prepared glass samples.

Measurement	Dy^{3+} Doped Concentration, mol%					
	0.0	**0.2**	**0.4**	**0.6**	**0.8**	**1.0**
Refractive index (n)	2.295	2.305	2.317	2.331	2.344	2.355
Reflection loss (R_L)	0.154	0.155	0.157	0.159	0.161	0.163
Molar refraction (R_m) (cm^{-3})	5.741	4.330	4.355	4.366	4.375	4.393
Oxygen packing density (OPD)	86.57	86.46	86.44	86.72	87.01	87.81
Optical basicity (Λ)	1.240	1.248	1.257	1.268	1.277	1.285
Optical electronegativity (χ)	0.919	0.903	0.885	0.863	0.845	0.829
Metallisation criterion (M)	0.412	0.410	0.407	0.403	0.400	0.397
Molar refractivity (R_M) (cm^{-3})	17.227	17.324	17.420	17.467	17.505	17.576
Molar polarizability (α_m) $\times10^{-24}$ (cm^{-3})	2.275	1.716	1.716	1.730	1.734	1.741
Dielectric constant (ε)	5.267	5.313	5.368	5.433	5.494	5.546
Optical dielectric constant	4.267	4.313	4.368	4.433	4.494	4.546
Electron polarizability (α_o)	2.672	2.687	2.703	2.723	2.739	2.753

Table 6 presented the optical properties of the glass samples. It is observed that the molar refractivity (R_M), reflection loss (R_L) and refractive index (n) has a significant influence on the polarizability (α_m) which demonstrates that the refractive index of the glasses does not solely depend on the density. It is known that the samples containing NBOs have great polarizability compared with samples containing bridging oxygen (BOs). The results presented here are in agreement with another work [38].

The theoretical optical basicity (Λ) is a calculation of oxygen's capacity to contribute a negative charge load in glasses. To classify the covalent/ionic ratios of the glass, the theoretical optical basicity may be used, because the increment in (Λ) values indicate the declining covalence. Table 6 indicates that the values of Λ are within the range 1.240–1.285 and found to increase with increasing Dy$_2$O$_3$ concentrations. Here, the increment in optical basicity values means the ability of oxide ions to transfer electrons in the cations surrounding them [7]. Figure 9 represents the decline in the metallization criterion with an increase in the Dy$_2$O$_3$ concentration. The obtained values confirm the non-metallic nature of the current glass samples [8]. From Table 3, the results show that the refractivity R_M, α_M, ε and optical dielectric constant increase with increasing Dy$_2$O$_3$, meaning an increase in NBOs inside the glass matrix.
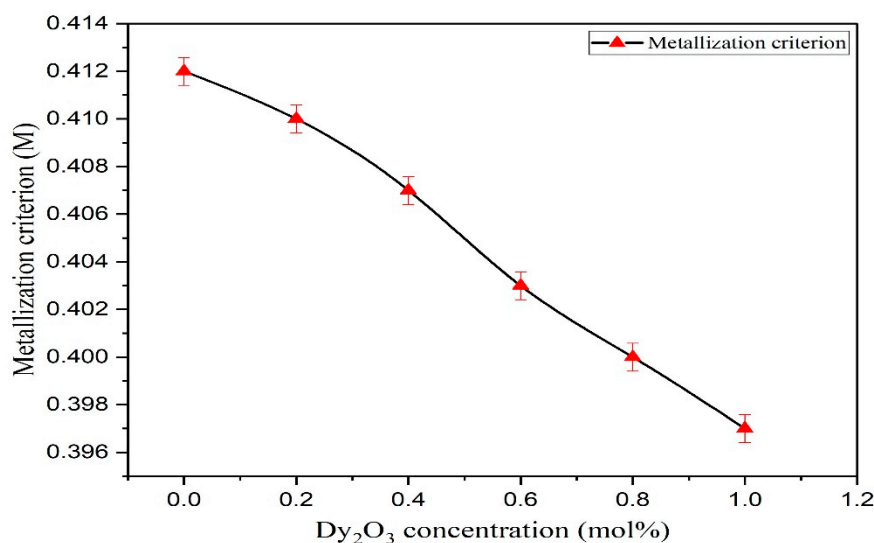
Figure 9. Variation in metallisation criterion with mol% Dy$_2$O$_3$.

The PL spectra for the current samples of various Dy^{3+}-doped compositions of (LAB) glass registered at room temperature in the wavelength region 420–720 nm below the excitation of the wavelength 375 nm are exhibited in Figure 10.
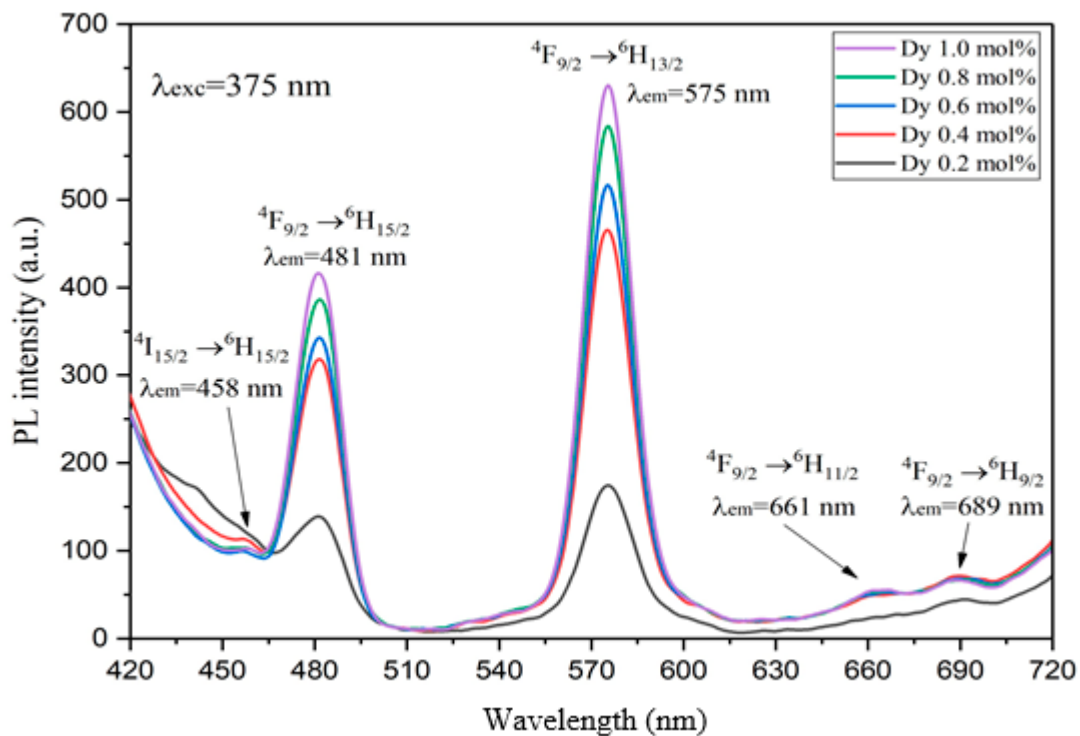

Figure 10. Emission spectra of LAB glasses doped with different concentrations (in mol%) of Dy^{3+} ions.

It was noticed that the emission peaks' intensity increased gradually as Dy^{3+} concentrations increased from 0.2 mol% to 1 mol%. The bands obtained in this present work are in agreement with the previous investigations [39]. Five emission peaks were spotted, containing two comparatively intense emission bands at nearly 481 and 575 nm, respectively, for the transitions $^4F_{9/2} \rightarrow \,^6H_{15/2}$ and $^4F_{9/2} \rightarrow \,^6H_{13/2}$, and three considerably feeble bands at almost 458, 661 and 689 nm corresponding to the transitions $^4I_{15/2} \rightarrow \,^6H_{15/2}$, $^4F_{9/2} \rightarrow \,^6H_{11/2}$ and $^4F_{9/2} \rightarrow \,^6H_{9/2}$, respectively [40]. These transitions are similar to other study, where the transition $^4I1_{5/2}$ level excites the Dy^{3+} ions at band 458 nm [12]. The excited Dy^{3+} ions populate the $^4F_{9/2}$ meta-stable state during rapid of non-radiative decay process due to the small energy gap between $4I_{15/2}$ and $^4F_{9/2}$ states [41]. The main higher band at 575 nm ($^4F_{9/2} \rightarrow \,^6H_{13/2}$) in the yellow range of the visible spectrum is a supersensitive transition following the selection rules ($\Delta J = \pm 2$ and $\Delta L = \pm 2$) [42].

In addition, the band at 481nm ($^4F_{9/2} \rightarrow \,^6H_{11/2}$), which is in the blue range, has low sensitivity to the host glass and is lower than the band at 575 nm that applies the selection rules ($\Delta J = \pm 3$). Therefore, the intensity of this transition is heavily impacted by the surrounding environment. Further to this, the weak intensity of emission bands appears at 661 nm ($^4F_{9/2} \rightarrow \,^6H_{11/2}$) and 689 nm ($^4F_{9/2} \rightarrow \,^6H_{9/2}$) is in the red range, which follows the selection rules ($\Delta J = \pm 1$) and ($\Delta J = 0$), $^6F_{11/2}$, respectively [33,43]. Spectroscopic and luminescence properties at 0.8 mol%-doped dysprosium ion are compared with other reported glass matrices and are found to be useful for yellow lighting applications in the visible spectral region. Those emissions, especially those at the visible light range, may increase the sensitivity of the composition and are apt to be used in several applications such as sensors and solar cells. Figure 11 illustrates a partial energy level diagram for the composition (LAB) of glass doped by several concentrations of Dy^{3+} ions. At excitation 375 nm, the Dy^{3+} ions were excited from the lower level of $^6H_{15/2}$ to higher-level $^6P_{7/2}$. After that, when the Dy^{3+} ions were decayed non-radiatively to $^6F_{9/2}$ level, the Dy^{3+} moved downward radiatively below the excitation of $^4I_{15/2}$. Prominent emission bands have

been identified: $^6H_{15/2}$ (blue), $^6H_{13/2}$ (yellow) and $^6H_{11/2}$—$^6H_{9/2}$ (red). The second part of this figure represents the absorption transition from the lower level ($^6H_{15/2}$) into the various energy levels $^6H_{11/2}$, $^6F_{11/2} + {}^6H_{9/2}$, $^6F_{9/2} + {}^6H_{7/2}$, $^6F_{7/2}$, $^6F_{5/2}$, $^4F_{9/2}$, $^6F_{3/2}$, $^4I_{15/2}$, $^4F_{7/2}$ and $^6P_{7/2}$. Hence the emission, absorption transitions, non-radiative, radiative energy transfer, cross-relaxation and ground state of the study samples are discussed.
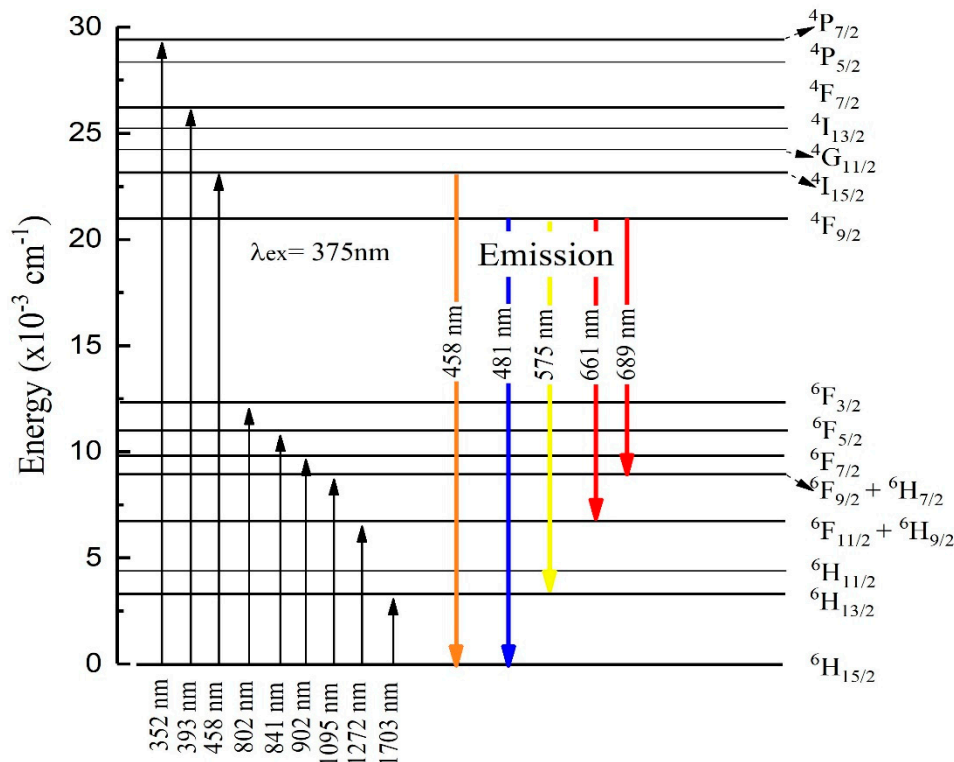
Figure 11. Partial energy levels of the RE ion showing distinct transitions.

4. Conclusions

In this study, new glass samples of the $23Li_2O$-$7.5Al_2O_3$-$(69.5 - x)$ B_2O_3: xDy_2O_3 system were prepared using the melt-quenching technique. The amorphous nature of glass samples was confirmed by the XRD analysis. Notably, the density and optical basicity increased with the presence of BO_4 tetrahedral units and, due to the structural changes, led to the decline in the direct and indirect energy gaps. From PL results, five emission bands were observed around at 458, 481, 575,661 and 689 nm, which are attributable to Dy^{3+} transitions of $^4I_{15/2} \rightarrow {}^6H_{15/2}$, $^4F_{9/2} \rightarrow {}^6H_{15/2}$, $^4F_{9/2} \rightarrow {}^6H_{13/2}$, $^4F_{9/2} \rightarrow {}^6H_{11/2}$ and $^4F_{9/2} \rightarrow {}^6H_{9/2}$, respectively. The 576 nm ($^4F_{9/2} \rightarrow {}^6H_{13/2}$) band is the largest. Hence, optical properties and other physical parameters, such as refractive index, density, molar volume, molar refractive, electrical polarisation and optical basicity, show a strong connexion with the speciation of dysprosium ions.

References

1. Anjaiah, J.; Laxmikanth, C.; Veeraiah, N.; Nalluri, V. Spectroscopic properties and luminescence behaviour of europium doped lithium borate glasses. *Phys. B Condens. Matter* **2014**, *454*, 148–156. [CrossRef]

2. Alajerami, Y.S.M.; Hashim, S.; Ghoshal, S.K.; Saleh, M.A.; Kadni, T.; Saripan, M.I.; Saripand, K.; Alzimamie, Z.; Bradley, D.A. The Effect of TiO_2 and MgO on the Thermoluminescence Properties of a Lithium Potassium Borate Glass System. *J. Phys. Chem. Solids* **2013**, *74*, 1816–1822. [CrossRef]

3. Okasha, A.; Abdelghany, A.; Marzouk, S. The influence of Ba^{2+} and Sr^{2+} ions with the Dy^{3+} ions on the optical properties of lead borate glasses: Experimental and Judd–Ofelt comparative study. *J. Mater. Res. Technol.* **2020**, *9*, 59–66. [CrossRef]

4. Ramteke, D.D.; Gedam, R.S. Study of Li_2O–B_2O_3–Dy_2O_3 glasses by impedance spectroscopy. *Solid State Ion.* **2014**, *258*, 82–87. [CrossRef]

5. Damodaraiah, S.; Prasad, V.R.; Babu, S.; Ratnakaram, Y. Structural and luminescence properties of Dy^{3+} doped bismuth phosphate glasses for greenish yellow light applications. *Opt. Mater.* **2017**, *67*, 14–24. [CrossRef]

6. Pawar, P.; Munishwar, S.; Gautam, S.; Gedam, R. Physical, thermal, structural and optical properties of Dy^{3+} doped lithium alumino-borate glasses for bright W-LED. *J. Lumin.* **2017**, *183*, 79–88. [CrossRef]

7. Chimalawong, P.; Kirdsiri, K.; Kaewkhao, J.; Limsuwan, P. Investigation on the Physical and Optical Properties of Dy^{3+} Doped Soda-Lime-Silicate Glasses. *Procedia Eng.* **2012**, *32*, 690–698. [CrossRef]

8. Yusof, N.N.; Ghoshal, S.K.; Omar, M.F. Physical, structural, optical and thermoluminescence behavior of Dy_2O_3 doped sodium magnesium borosilicate glasses. *Results Phys.* **2019**, *12*, 827–839.

9. Anwar, A.; Zulfiqar, S.; Yousuf, M.A.; Ragab, S.A.; Khan, M.A.; Shakir, I.; Warsi, M.F. Impact of rare earth Dy^{+3} cations on the various parameters of nanocrystalline nickel spinel ferrite. *J. Mater. Res. Technol.* **2020**, *9*, 5313–5325. [CrossRef]

10. Mhareb, M.; Hashim, S.; Ghoshal, S.; Alajerami, Y.; Bqoor, M.J.; Hamdan, A.I.; Saleh, M.A.; Karim, M.K.A. Effect of Dy_2O_3 impurities on the physical, optical and thermoluminescence properties of lithium borate glass. *J. Lumin.* **2016**, *177*, 366–372. [CrossRef]

11. Mhareb, M.; Hashim, S.; Ghoshal, S.K.; Alajerami, Y.S.M.; Saleh, M.A.; Azizan, S.A.B.; Razak, N.A.B.; Karim, M.K.A. Influences of dysprosium and phosphorous oxides co-doping on thermoluminescence features and kinetic parameters of lithium magnesium borate glass. *J. Radioanal. Nucl. Chem.* **2015**, *305*, 469–477. [CrossRef]

12. Pawar, P.P.; Munishwar, S.R.; Gautam, S.; Gedam, R.S. Structural and photoluminescence properties of Dy^{3+} doped different modifier oxide-based lithium borate glasses. *J. Lumin.* **2012**, *132*, 2984–2991.

13. Zelati, A.; Amirabadizadeh, A.; Hosseini, A. A facile approach to synthesize dysprosium oxide nanoparticles. *Int. J. Ind. Chem.* **2014**, *5*, 69–75. [CrossRef]

14. Khan, I.; Rooh, G.; Rajaramakrishna, R.; Srisittipokakun, N.; Kim, H.J.; Kaewkhao, J.; Ruangtaweep, Y. Photoluminescence Properties of Dy^{3+} Ion-Doped Li_2O-PbO-Gd_2O_3-SiO_2 Glasses for White Light Application. *Braz. J. Phys.* **2019**, *49*, 605–614. [CrossRef]

15. Mhareb, M.; Almessiere, M.; Sayyed, M.; Alajerami, Y. Physical, structural, optical and photons attenuation attributes of lithium-magnesium-borate glasses: Role of Tm_2O_3 doping. *Optik* **2019**, *182*, 821–831. [CrossRef]

16. Kamaruddin, W.; Rohani, M.; Sahar, M.; Liu, H.; Sang, Y. Synthesis and characterization of lithium niobium borate glasses containing neodymium. *J. Rare Earths* **2016**, *34*, 1199–1205. [CrossRef]

17. Ichoja, A.; Hashim, S.; Ghoshal, S.; Hashim, I.H.; Omar, R. Physical, structural and optical studies on magnesium borate glasses doped with dysprosium ion. *J. Rare Earths* **2018**, *36*, 1264–1271. [CrossRef]

18. Effendy, N.; Wahab, Z.A.; Aziz, S.A.; Matori, K.A.; Zaid, M.H.M.; Rashid, S.S.A.; Nuraidayani, E.; Abdul, W.Z.; Hj., A.A.S.; Amin, M.K.; et al. Characterization and optical properties of erbium oxide doped ZnO–SLS glass for potential optical and optoelectronic materials. *Mater. Express* **2017**, *7*, 59–65. [CrossRef]

19. Shaaban, K.; El-Maaref, A.; Abdelawwad, M.; Saddeek, Y.B.; Wilke, H.; Hillmer, H. Spectroscopic properties and Judd-Ofelt analysis of Dy^{3+} ions in molybdenum borosilicate glasses. *J. Lumin.* **2018**, *196*, 477–484. [CrossRef]

20. Babu, M.R.; Babu, A.M.; Moorthy, L.R. Structural and optical properties of Nd^{3+}-doped lead borosilicate glasses for broadband laser amplification. *Int. J. Appl. Eng. Res.* **2018**, *13*, 7692–7700.

21. Bhatia, B.; Meena, S.L.; Parihar, V.; Poonia, M. Optical Basicity and Polarizability of Nd^{3+}-Doped Bismuth Borate Glasses. *New J. Glas. Ceram.* **2015**, *5*, 44–52. [CrossRef]

22. Gedam, R.; Ramteke, D. Influence of CeO$_2$ addition on the electrical and optical properties of lithium borate glasses. *J. Phys. Chem. Solids* **2013**, *74*, 1399–1402. [CrossRef]

23. Hasnimulyati, L.; Halimah, M.K.; Zakaria, A.; Halim, S.A.; Ishak, M.; Eevon, C. Structural and optical properties of Tm$_2$O$_3$-doped zinc borotellurite glass system. *J. Ovonic Res.* **2016**, *12*, 291–299.

24. Kundu, V.; Dhiman, R.L.; Maan, A.S.; Goyal, D.R.; Garg, A.B.; Mittal, R.; Mukhopadhyay, R. Optical Properties of Alkaline Earth Ions Doped Bismuth Borate Glasses. *AIP Conf. Proc.* **2011**, *1349*, 545. [CrossRef]

25. Kaur, P.; Singh, K.; Kurudirek, M.; Thakur, S. Study of environment friendly bismuth incorporated lithium borate glass system for structural, gamma-ray and fast neutron shielding properties. *Spectrochim. Acta Part A Mol. Biomol. Spectrosc.* **2019**, *223*, 117309. [CrossRef]

26. Algradee, M.A.; Sultan, M.; Samir, O.M.; Alwany, A.E.B. Electronic polarizability, optical basicity and interaction parameter for Nd$_2$O$_3$ doped lithium–zinc–phosphate glasses. *Appl. Phys. A Mate. Sci. Process.* **2017**, *123*, 524. [CrossRef]

27. Pawar, P.; Munishwar, S.R.; Gedam, R. Eu$_2$O$_3$ doped bright orange-red luminescent lithium alumino-borate glasses for solid state lighting. *J. Lumin.* **2018**, *200*, 216–224. [CrossRef]

28. Deepa, A.V.; Priya, M.; Suresh, S. Influence of Samarium Oxide ions on structural and optical properties of borate glasses. *Sci. Res. Essays* **2016**, *11*, 57–63. [CrossRef]

29. Chandrasekhar, M.; Nagabhushana, H.; SudheerKumar, K.; Dhananjaya, N.; Sharma, S.; Kavyashree, D.; Shivakumara, C.; Nagabhushana, B. Comparison of structural and luminescence properties of Dy$_2$O$_3$ nanopowders synthesized by co-precipitation and green combustion routes. *Mater. Res. Bull.* **2014**, *55*, 237–245. [CrossRef]

30. Ramteke, D.; Ganvir, V.; Munishwar, S.R.; Gedam, R. Concentration Effect of Sm^{3+} Ions on Structural and Luminescence Properties of Lithium Borate Glasses. *Phys. Procedia* **2015**, *76*, 25–30. [CrossRef]

31. Pawar, P.; Munishwar, S.; Gedam, R. Intense white light luminescent Dy^{3+} doped lithium borate glasses for W-LED: A correlation between physical, thermal, structural and optical properties. *Solid State Sci.* **2017**, *64*, 41–50. [CrossRef]

32. Shamshad, L.; Rooh, G.; Kirdsiri, K.; Srisittipokakun, N.; Damdee, B.; Kim, H.; Kaewkhao, J. Photoluminescence and white light generation behavior of lithium gadolinium silicoborate glasses. *J. Alloys Compd.* **2017**, *695*, 2347–2355. [CrossRef]

33. Deopa, N.; Rao, A. Photoluminescence and energy transfer studies of Dy^{3+} ions doped lithium lead alumino borate glasses for w-LED and laser applications. *J. Lumin.* **2017**, *192*, 832–841. [CrossRef]

34. Dawaud, R.S.E.S.; Hashim, S.; Alajerami, Y.; Mhareb, M.; Tamchek, N. Optical and structural properties of lithium sodium borate glasses doped Dy^{3+} ions. *J. Mol. Struct.* **2014**, *1075*, 113–117. [CrossRef]

35. Pawar, P.; Munishwar, S.; Ramteke, D.; Gedam, R. Physical, structural, thermal and spectroscopic investigation of Sm$_2$O$_3$ doped LAB glasses for orange LED. *J. Lumin.* **2019**, *208*, 443–452. [CrossRef]

36. Azizan, S.A.; Hashim, S.; Razak, N.A.; Mhareb, M.H.A.; Alajerami, Y.S.M.; Tamchek, N. Physical and optical properties of Dy^{3+}: Li$_2$O–K$_2$O–B$_2$O$_3$ glasses. *J. Mol. Struct.* **2014**, *1076*, 20–25. [CrossRef]

37. Obayes, H.K.; Hussin, R.; Wagiran, H.; Saeed, M. Strontium ion concentration effects on structural and spectral properties of Li$_4$Sr(BO$_3$)$_3$ glass. *J. Non-Cryst. Solids* **2015**, *427*, 83–90. [CrossRef]

38. Yusof, N.N.; Ghoshal, S.; Omar, M.F. Modified absorption attributes of neodymium doped magnesium-zinc-sulfophosphate glass. *Malays. J. Fundam. Appl. Sci.* **2017**, *13*, 258–262. [CrossRef]

39. Bulus, I.; Dalhatu, S.A.; Isah, M.; Hussin, R.; Soje, E.A. Structural and Luminescence Characterization of Lithium-Borosulfophosphate Glasses Containing Dysprosium Ions. *Sci. World J.* **2017**, *12*, 98–101.

40. Rani, P.R.; Venkateswarlu, M.; Mahamuda, S.; Swapna, K.; Deopa, N.; Rao, A. Spectroscopic studies of Dy^{3+} ions doped barium lead alumino fluoro borate glasses. *J. Alloys Compd.* **2019**, *787*, 503–518. [CrossRef]

41. Babu, A.M.; Jamalaiah, B.; Kumar, J.S.; Sasikala, T.; Moorthy, L.R. Spectroscopic and photoluminescence properties of Dy^{3+}-doped lead tungsten tellurite glasses for laser materials. *J. Alloys Compd.* **2011**, *509*, 457–462. [CrossRef]

42. Shasmal, N.; Karmakar, B. White light-emitting Dy^{3+}-doped transparent chloroborosilicate glass: Synthesis and optical properties. *J. Asian Ceram. Soc.* **2018**, *7*, 42–52. [CrossRef]

43. Deopa, N.; Rao, A.; Gupta, M.; Prakash, G.V. Spectroscopic investigations of Nd^{3+} doped Lithium Lead Alumino Borate glasses for 1.06 µm laser applications. *Opt. Mater.* **2018**, *75*, 127–134. [CrossRef]

Publisher's Note: MDPI stays neutral with regard to jurisdictional claims in published maps and institutional affiliations.